Electronic Supplementary Information

A new fluorescence turn-on chemosensor for nanomolar detection of Al^{3+} constructed from pyridine-pyrazole system

Barnali Naskar,[‡a] Kinsuk Das,[‡b] Ramij R. Mondal,[a] Dilip K. Maiti,[a] Alberto Requena,[c] José Pedro Cerón-Carrasco,[d] Chandraday Prodhan,[e] Keya Chaudhuri,[e] and Sanchita Goswami*[a]

[a]Department of Chemistry, University of Calcutta, 92, A. P. C. Road, Kolkata – 700009, India
E-mail: sgchem@caluniv.ac.in

[b]Department of Chemistry, Chandernagore College, Hooghly 712136, West Bengal, India

[c]Departamento de Química Física, Facultad de Química, Universidad de Murcia, 30100 Murcia, Spain

[d]Bioinformatics and High Performance Computing Research Group (BIO-HPC), Universidad Católica San Antonio de Murcia (UCAM), 30107 Murcia, Spain

[e]Molecular & Human Genetics Division, CSIR–Indian Institute of Chemical Biology, 4 Raja S.C. Mallick Road, Kolkata–700032, India

‡ These authors contributed equally to this article.

Contents of the Supporting Information

1. Characterization and Structural Data *Pages*

2. Photophysical Characterization

3. Theoretical Data

4. Cell Study

1. Characterization and Structural Data.

^{1}H and ^{13}C−NMR spectra: Hmppc was dissolved in d_6– DMSO and recorded with TMS as internal standard on a Bruker, AV 300 Supercon Digital NMR system.

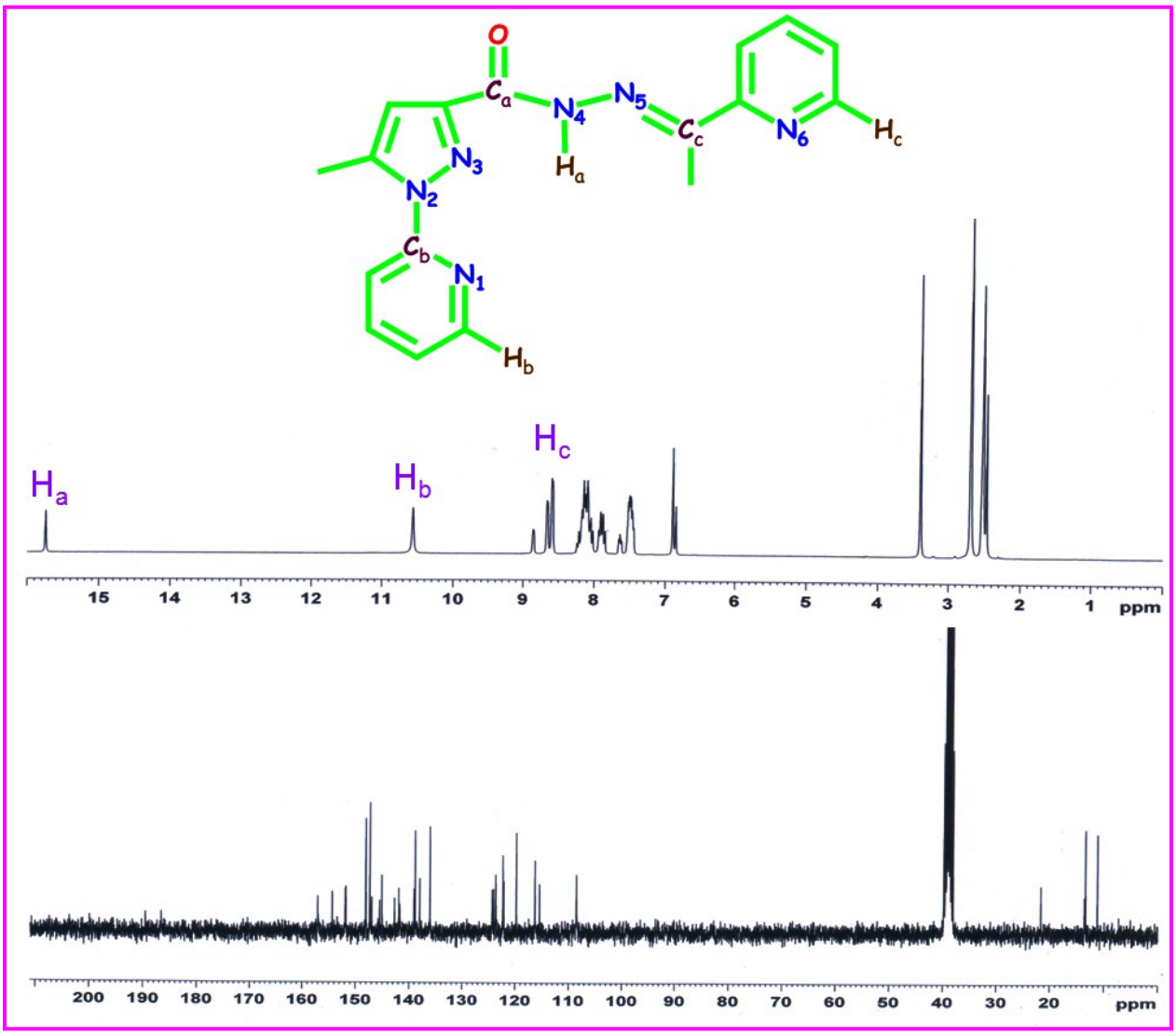

Figure S1. ^{1}H and ^{13}C−NMR spectrum of chemosensor (**Hmppc**).

1. Characterization and Structural Data.

FT–IR spectroscopy: Fourier transform infrared (FT−IR) spectra were recorded with a Perkin−Elmer RXI FT−IR spectrophotometer using the reflectance technique (4000−400 cm^{-1}). Samples were prepared as KBr disks.

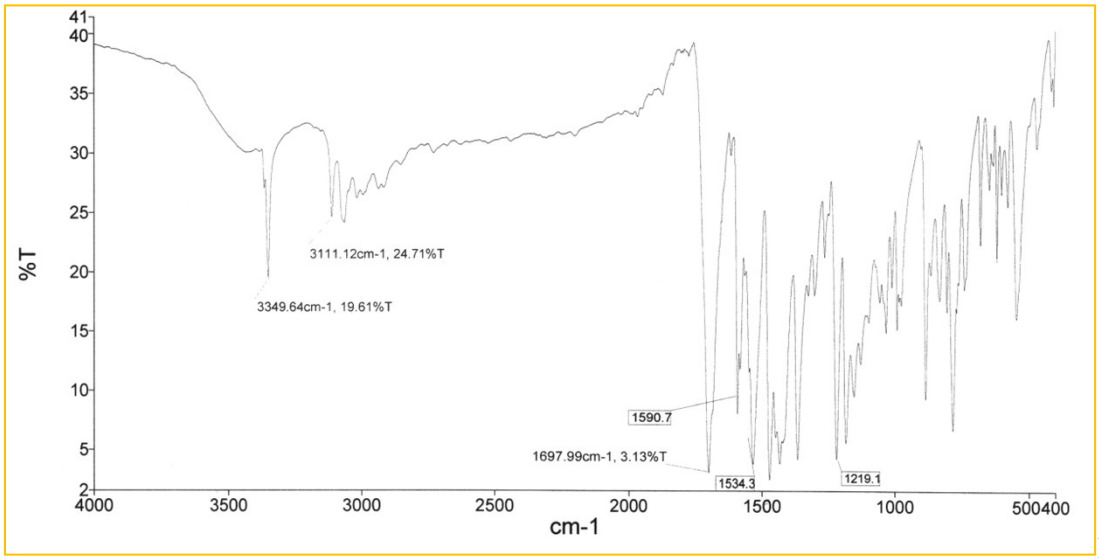

Hmppc

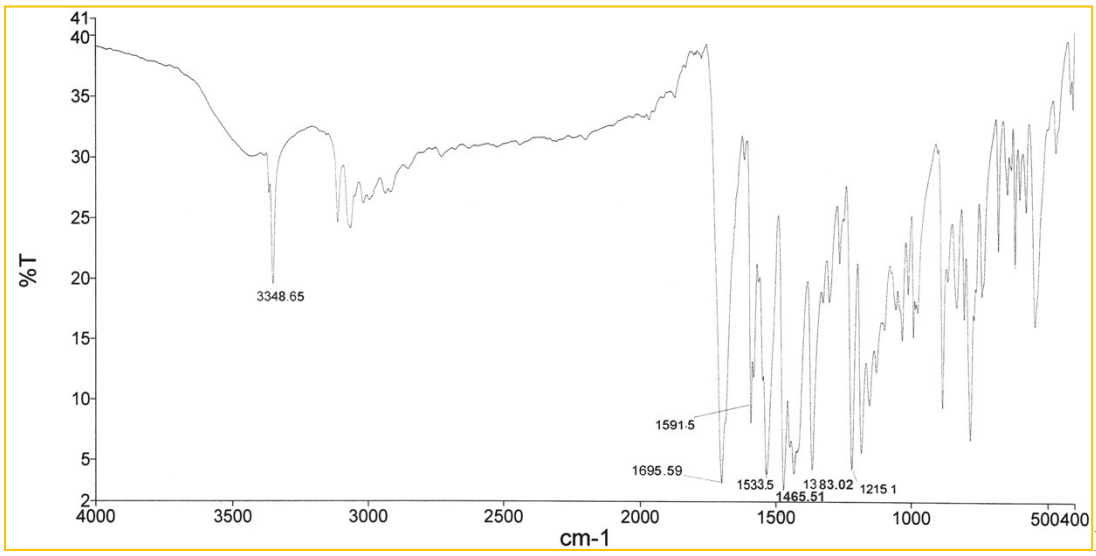

Hmppc-Al^{3+}

Figure S2. FT−IR Spectrum of chemosensor (**Hmppc**) and Aluminium complex (**Hmppc–Al^{3+}**).

1. Characterization and Structural Data.

Electrospray mass spectra (ESI-MS) were recorded on Qtof Micro YA263 mass spectrometer dissolving the samples in LC–MS quality MeOH.

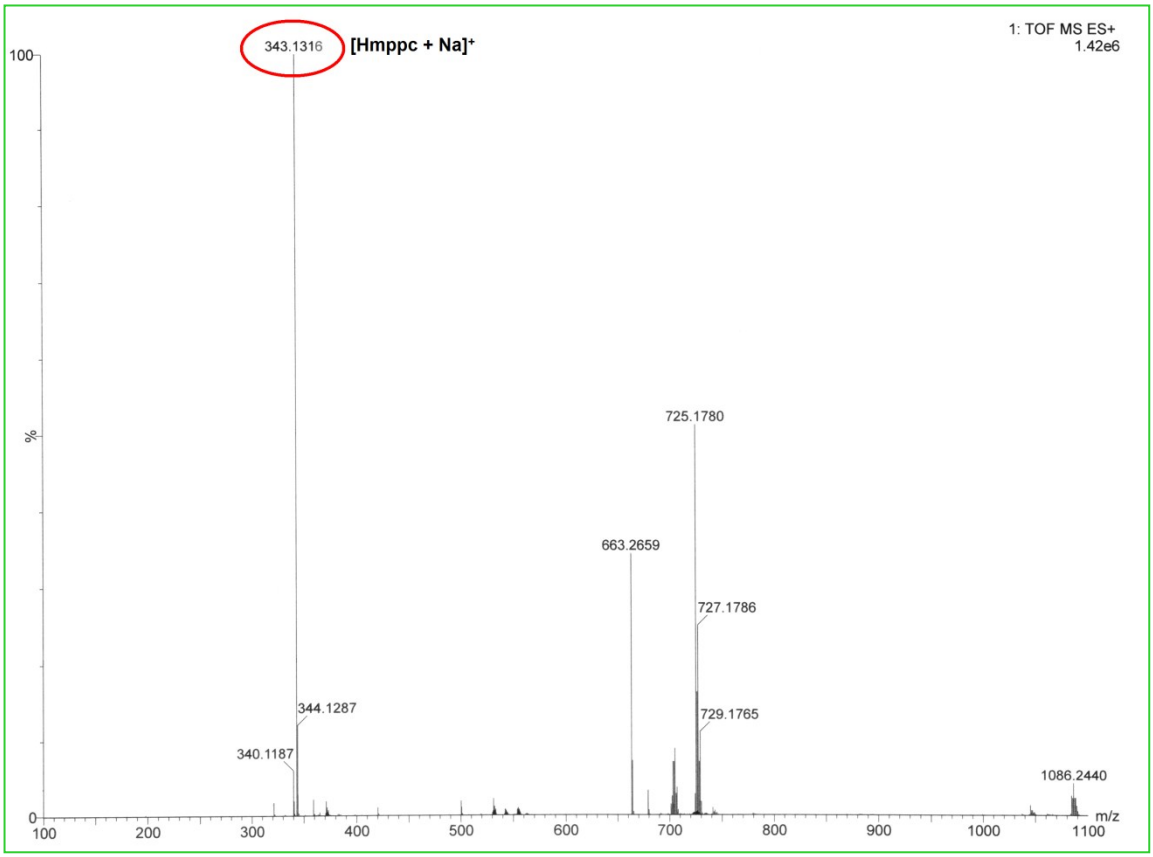

Hmppc

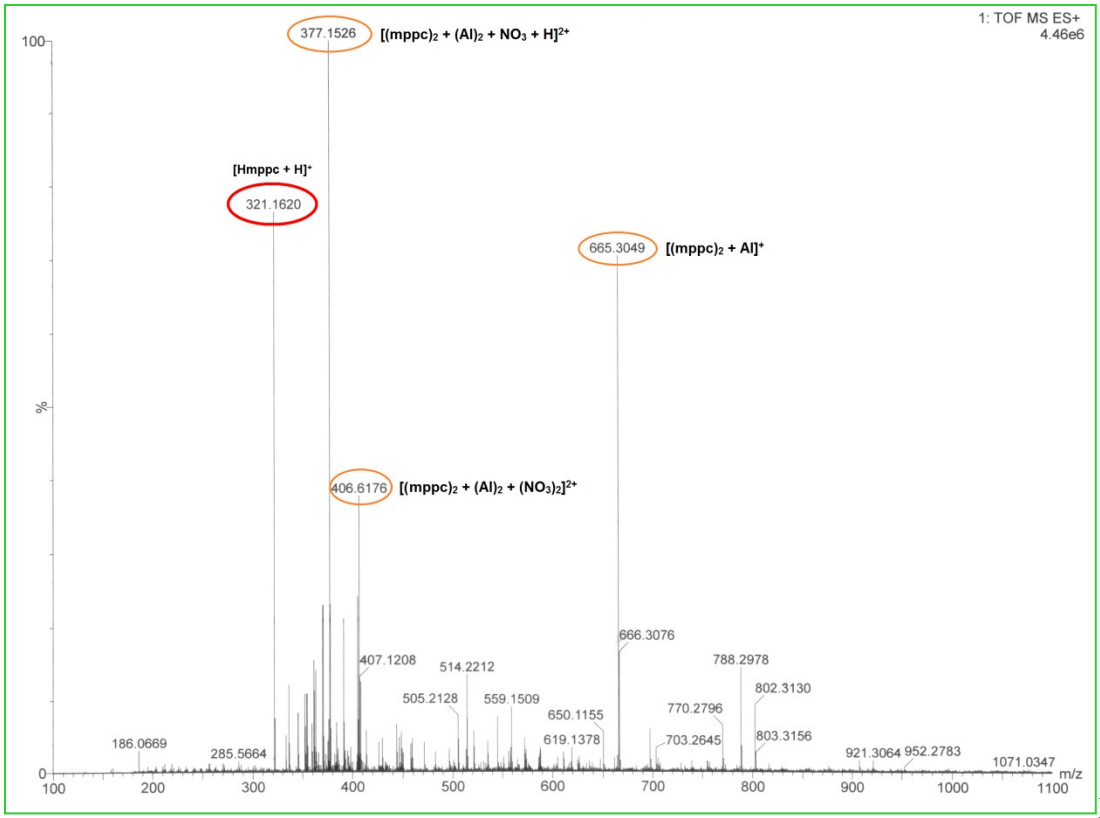

Hmppc-Al^{3+}

Figure S3. ESI–MS of **Hmppc** and Aluminium complex (**Hmppc–Al^{3+}**).

1. Characterization and Structural Data.

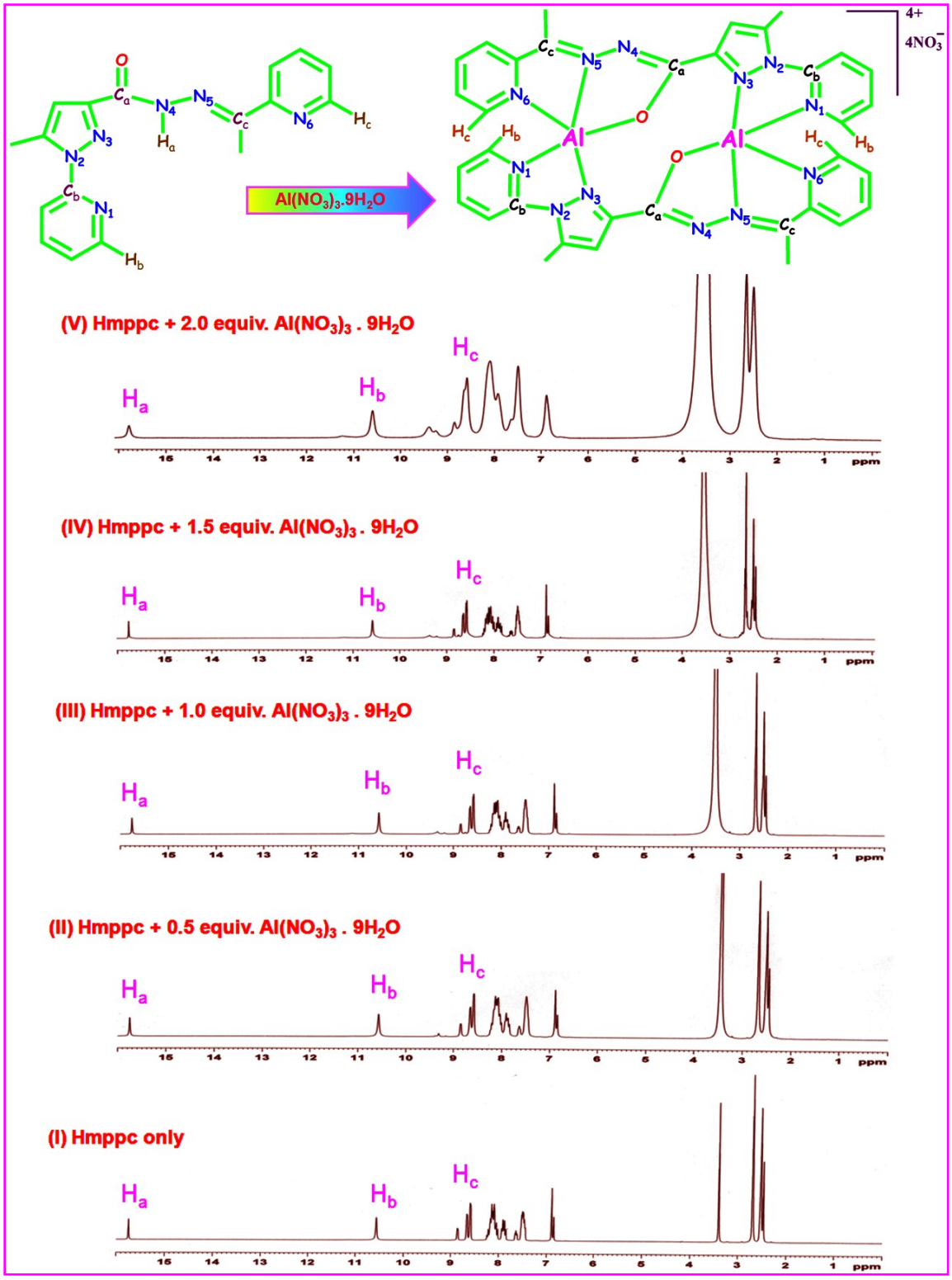

Figure S4. ^{1}H−NMR titration of **Hmppc** with $Al(NO_3)_3.9H_2O$ in DMSO−d_6 solution.

1. Characterization and Structural Data.

Table S1. ^{1}H and ^{13}C−NMR shift data of NMR titration experiment.

^{1}H						
Proton label	**Free Hmppc (ppm) (A)**	**Hmppc + 0.5 equiv. $Al(NO_3)_3.9H_2O$ (ppm) (B)**	**Hmppc + 1.0 equiv. $Al(NO_3)_3.9H_2O$ (ppm) (C)**	**Hmppc + 1.5 equiv. $Al(NO_3)_3.9H_2O$ (ppm) (D)**	**Hmppc + 2.0 equiv. $Al(NO_3)_3.9H_2O$ (ppm) (E)**	**Shift (E−A) (ppm)**
H_a	15.742	Vanish	Vanish	Vanish	Vanish	−
H_b	10.567	10.576	10.581	10.588	10.604	0.037 **downfield**
H_c	8.861	8.849	8.843	8.661	8.854	-0.007 **upfield**
^{13}C						
C_a	157.06	157.10	157.13	157.28	157.28	0.22 **downfield**
C_b	154.35	154.32	154.28	154.26	154.24	-0.11 **upfield**
C_c	151.93	151.92	151.86	151.78	151.54	-0.39 **upfield**

2. Photophysical Characterization.

Benesi–Hildebrand plot in UV–Vis spectroscopy.

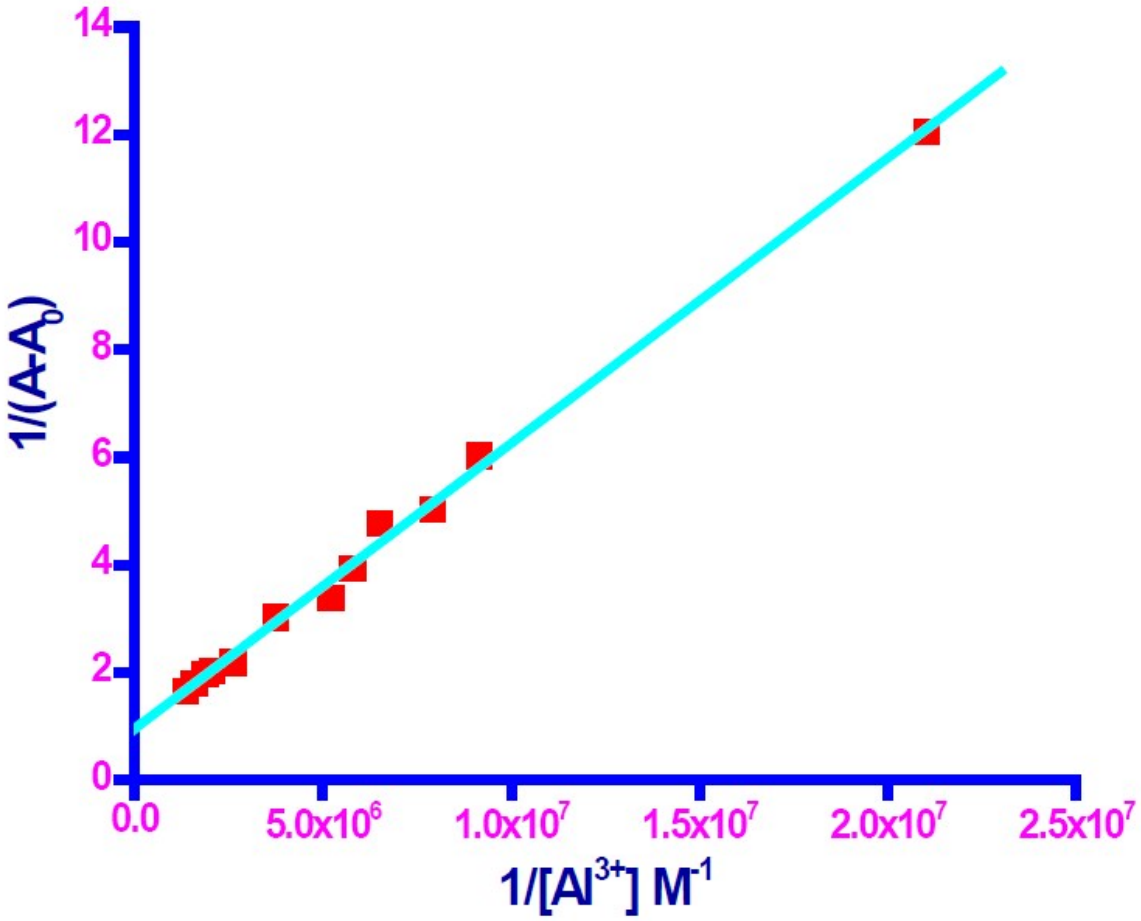

Figure S5. Benesi–Hildebrand plot of absorbance titration curve of **Hmppc** with $[Al^{3+}]$ at 356 nm.

2. Photophysical Characterization.

Benesi–Hildebrand plot in emission spectroscopy.

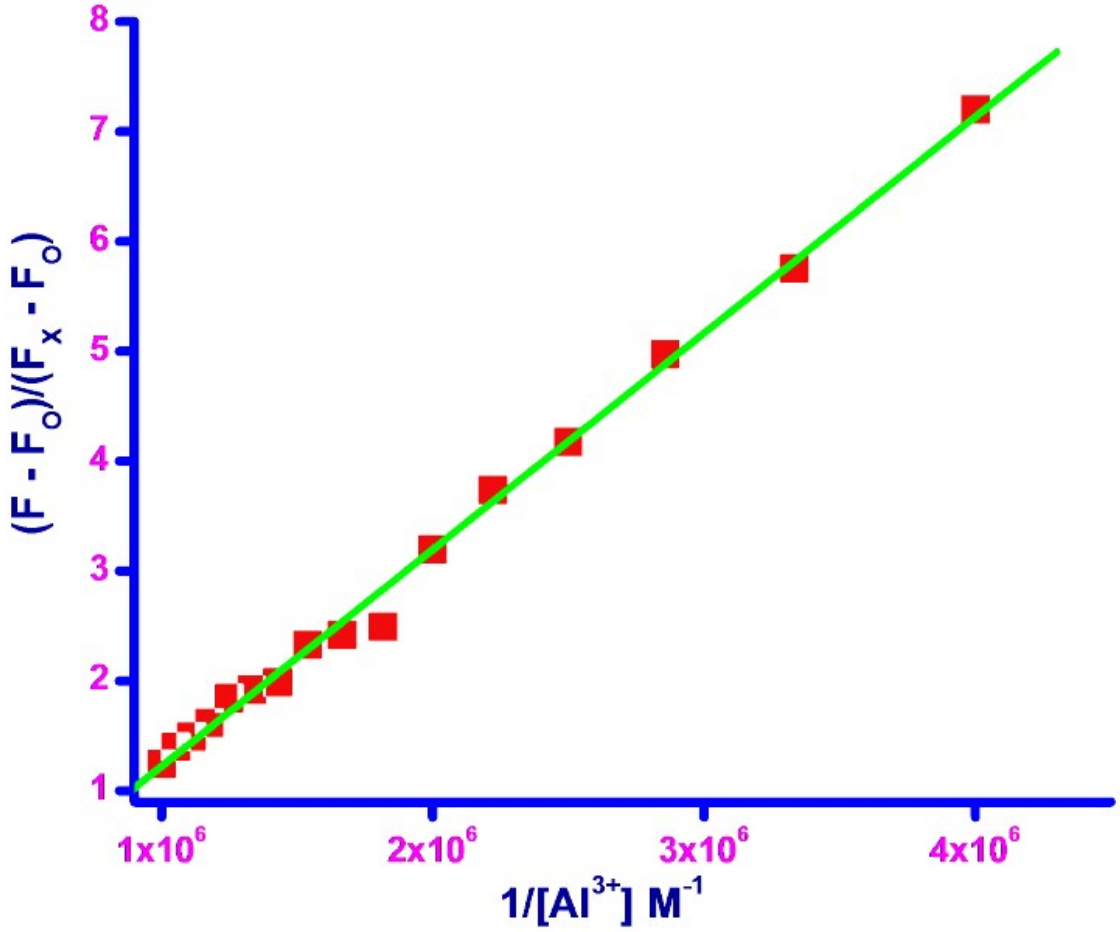

Figure S6. Benesi–Hildebrand plot $(F - F_0) / (F_x - F_0)$ vs. $1/ [Al^{3+}]$ for complexation between **Hmppc** and Al^{3+} derived from emission titration curve at 450 nm.

2. Photophysical Characterization.

Job′s plot for determination of stoichiometry of Al^{3+}: **Hmppc** complex in solution.

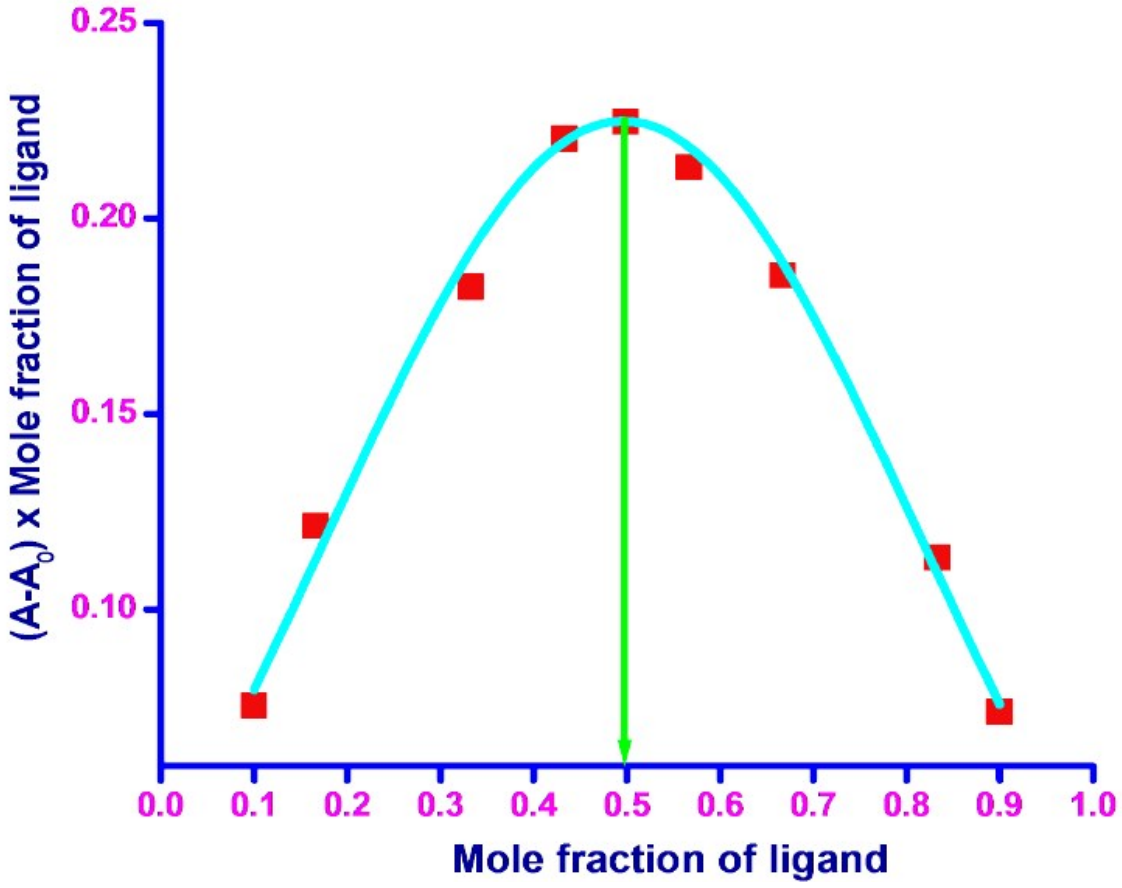

Figure S7. Job′s plot for the identification of **Hmppc–Al^{3+}** (1:1) complex stoichiometry using absorbance values.

2. Photophysical Characterization.

Detection limit calculation in emission spectroscopy.

The limit of detection (LOD) of **Hmppc**–Al^{3+} was measured on the basis of fluorescence titration measurement. The detection limit was calculated using the following equation:

$$LOD = K \times \frac{\sigma}{S}$$

where $K = 2$ or 3 (we take 3 in this case), 'σ' is the standard deviation of the blank solution and 'S' is the slope between the ratio of emission intensity *versus* [Al^{3+}].

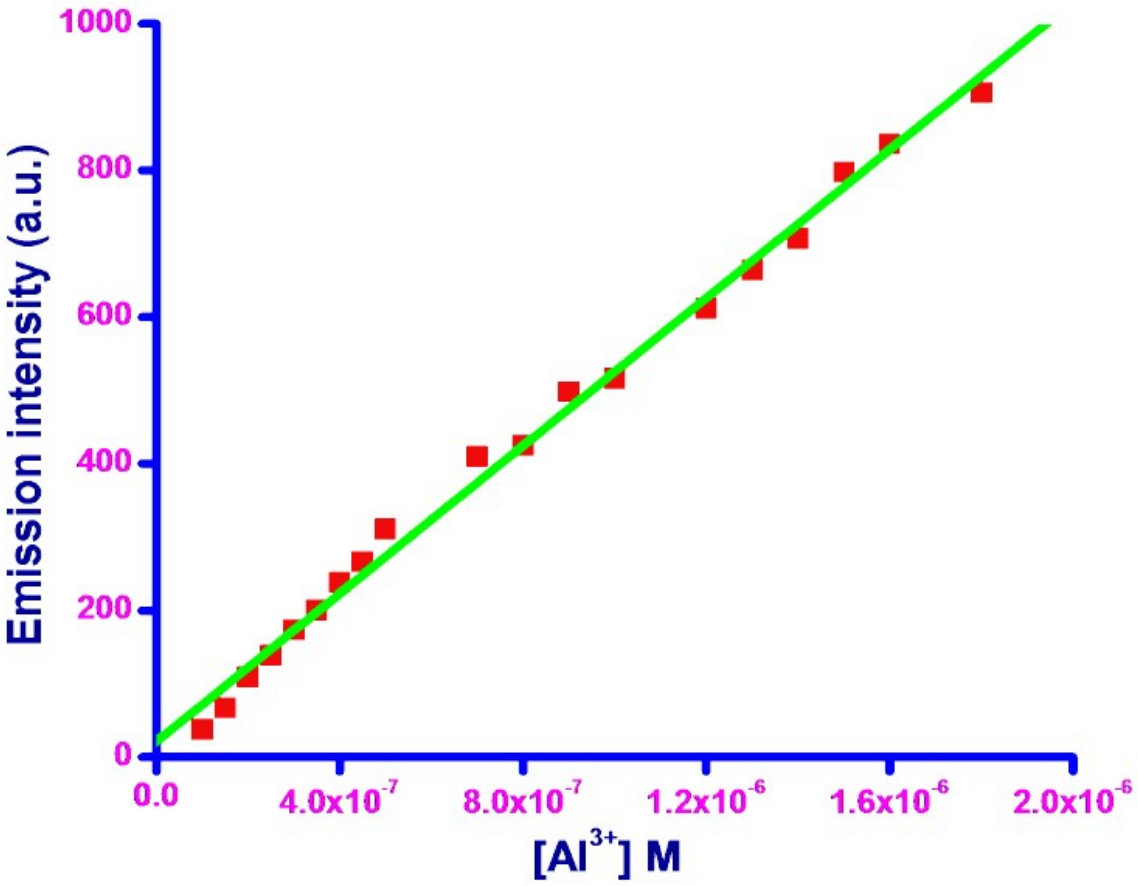

Figure S8. Determination of the detection limit of Al^{3+} by **Hmppc** in DMSO/H_2O (2:8, v/v) HEPES buffer (pH = 7.4) solution at 450 nm.

2. Photophysical Characterization.

Reversibility studies in emission spectroscopy.

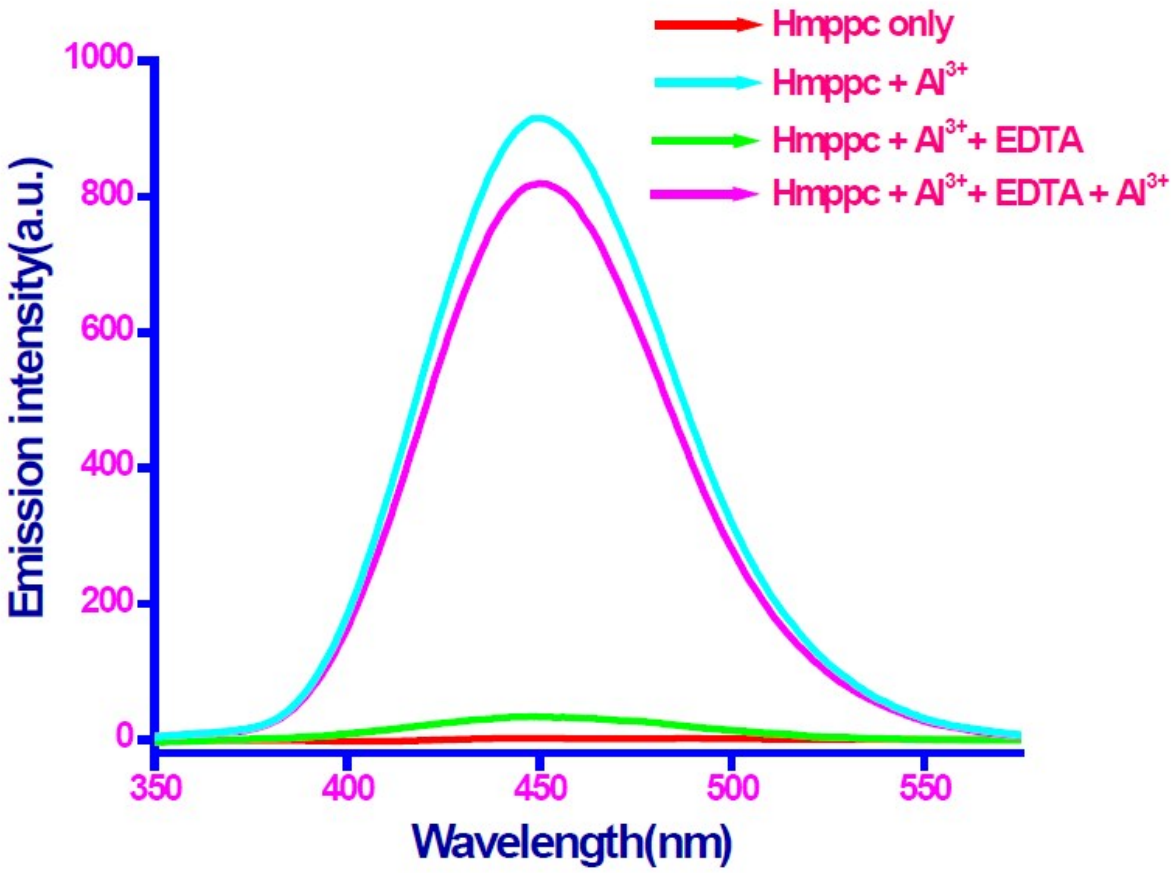

Figure S9. Fluorescence emission spectra of **Hmppc** in the presence of Al^{3+} ion followed by addition of EDTA (λ_{ex}=300 nm, λ_{em}=450 nm).

2. Photophysical Characterization.

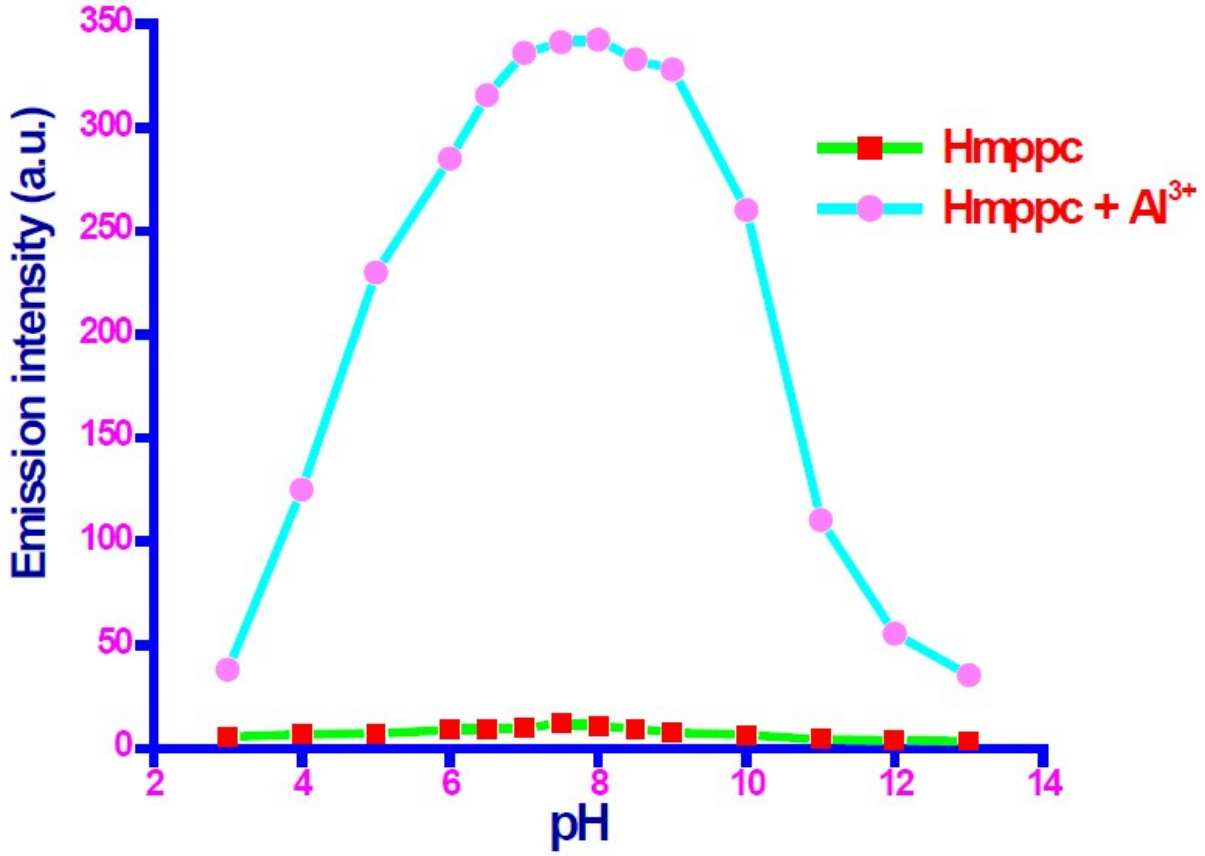

Figure S10. Emission intensity of probe **Hmppc** (5×10^{-7} M) in absence and in presence of Al^{3+} as a function of pH values in aqueous DMSO solution at 450 nm.

Table S2. Fluorescence lifetime measurement of chemosensor (**Hmppc**) and the presence of Al^{3+} ion in solution.

	φ_f	τ_{av} (ns)	K_r ($\times10^9$) S^{-1}	K_{nr} ($\times10^9$) S^{-1}	$\chi2$
Hmppc	0.051	2.32	0.022	0.409	1.012
Hmppc +Al^{3+}	0.610	3.45	0.177	0.113	1.043

3. Theoretical Data.

All quantum mechanical calculations were performed with in the density functional theory (DFT) approach by using the Gaussian09 suite of programs[S1] and the Jaguar code as implemented in the Schrödinger Release 2016-4.[S2, S3] The selected level of theory combines the parameter-free PBE0 hybrid functional to the 6-31++G (d, p) basis set for all atoms.[S4, S5] The used that computational protocol has been shown to correctly describe the absorption and emission spectra of a wide panel of organic molecules, including metal probes.[S6] The geometries of **Hmppc** as both metal-free and complexed to Al^{3+} were fully optimized (Fig. S11†). Additional vibrational calculations were conducted to confirm that the optimization processes reach true minima in the potential energy surface rather than saddel points (i.e., no imaginary frequencies). The vertical absorption energies are computed within the time-dependent DFT (TD-DFT) framework, a theoretical approach able to provide realible UV-vis spectra at a well balanced computational cost.[S7] As for the emission spectra is concerns, additional optimizations were carried out for the first excited state. The obtained theoretical spectra (Fig. S12† and Fig. S13†) match with the experimentally measure signatures, which confirm the ability of the DFT calculations to assess the nature of the excited states involved in the optical changes of **Hmppc** depending on the absence or presence of Al^{3+} in the medium.

3. Theoretical Data.

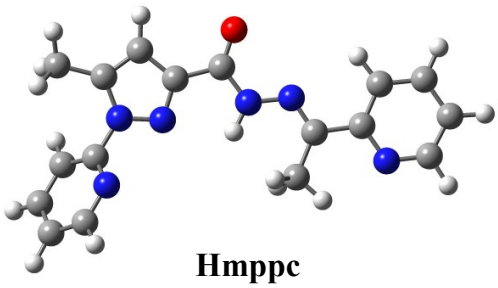

Hmppc

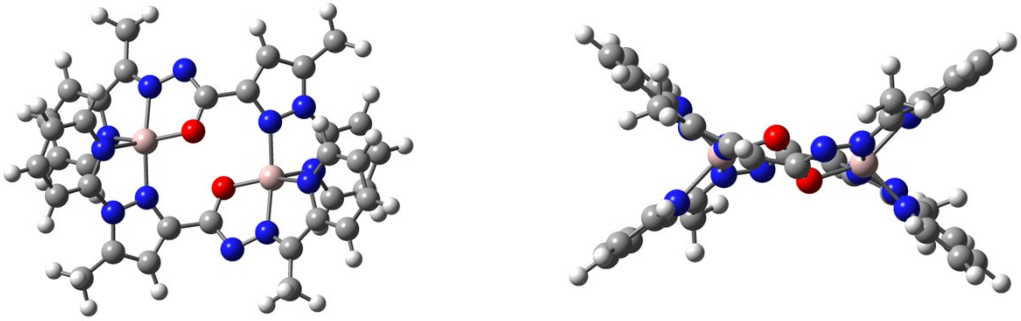

Front (left) and side (right) view for the optimized **Hmppc** aluminium complex.

Figure S11. DFT optimized structures of probe **Hmppc** in absence (up panel) and in presence (down panel) of Al^{3+} ions. Color scheme: carbons are displayed in grey, hydrogen in white, nitrogen in blue, oxygen in red and aluminium centers in light pink.

3. Theoretical Data.

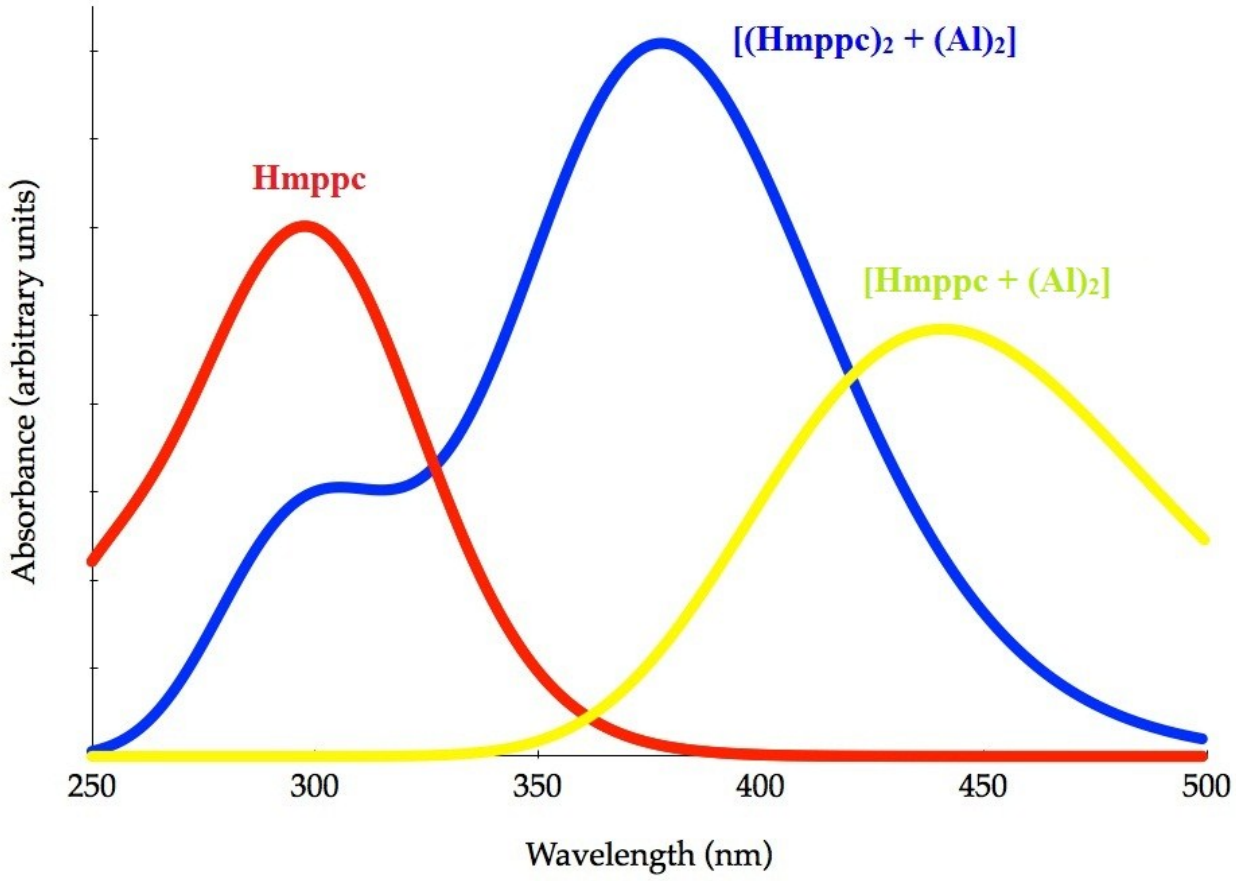

Figure S12. Computed TD-DFT absorption spectra of probe **Hmppc** in absence (red line) and in presence of Al^{3+} (blue and yellow line).

3. Theoretical Data.

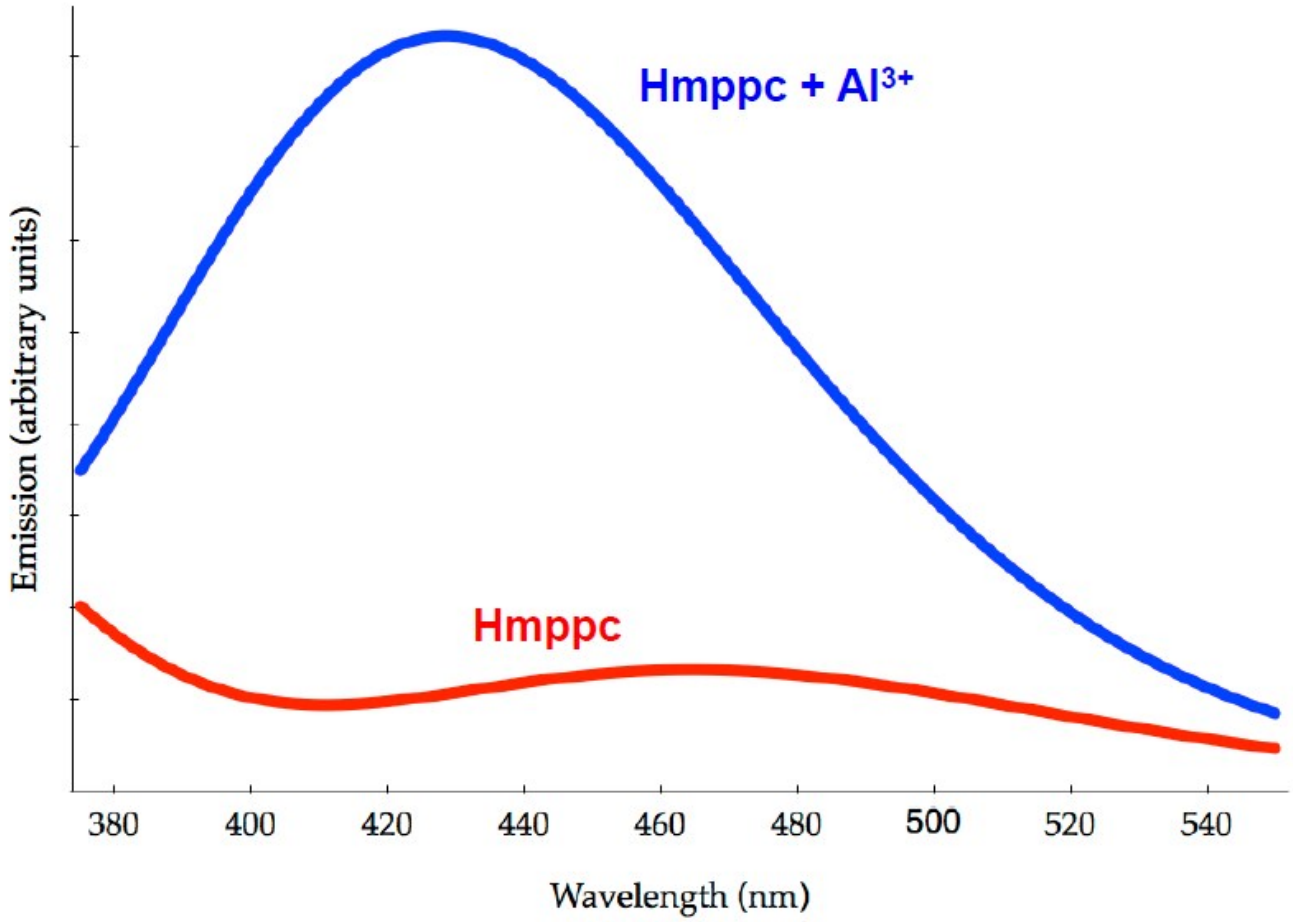

Figure S13. Computed TD-DFT emission spectra of probe **Hmppc** in absence (red line) and in presence of Al^{3+} (blue line).

3. Theoretical Data.

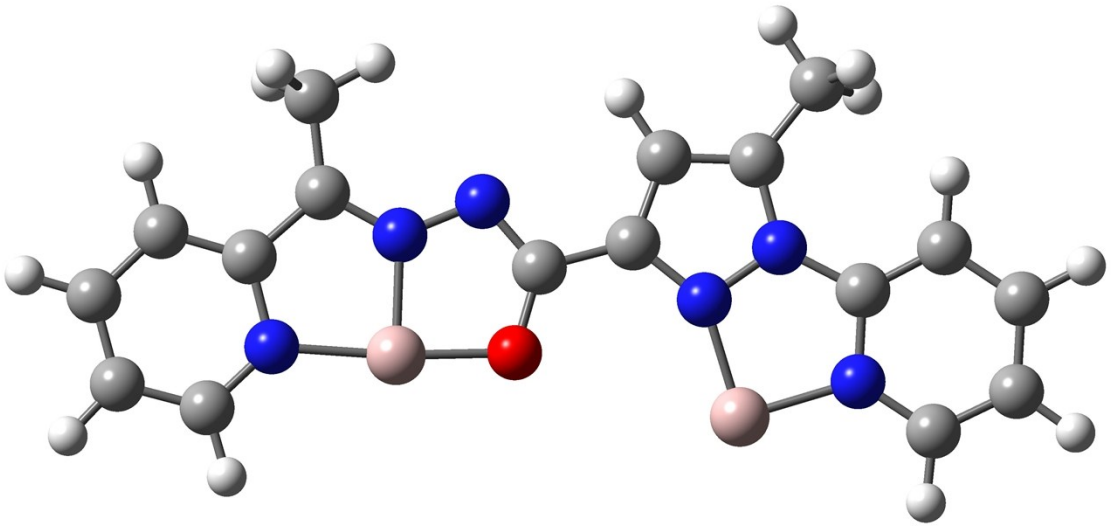

Figure S14. DFT optimized structures of the Hmppc-Al_2 complex.

3. Theoretical Data.

References for the computational methods:

[S1] Gaussian 09, Revision **D.01**, M. J. Frisch, G. W.Trucks, H. B. Schlegel, G. E. Scuseria, M. A. Robb, J. R. Cheeseman, G. Scalmani, V. Barone, B. Mennucci, G. A. Petersson, H. Nakatsuji, M. Caricato, X. Li, H. P. Hratchian, A. F. Izmaylov, J. Bloino, G. Zheng, J. L. Sonnenberg, M. Hada, M. Ehara, K. Toyota, R. Fukuda, J. Hasegawa, M. Ishida, T. Nakajima, Y. Honda, O. Kitao, H. Nakai, T. Vreven, Jr. Montgomery, J. E. Peralta, F. Ogliaro, M. Bearpark, J. J. Heyd, E. Brothers, K. N. Kudin, V. N. Staroverov, R. Kobayashi, J. Normand, K. Raghavachari, A. Rendell, J. C. Burant, S. S. Iyengar, J. Tomasi, M. Cossi, N. Rega, J. M. Millam, M. Klene, J. E. Knox, J. B. Cross, V. Bakken, C. Adamo, J. Jaramillo, R. Gomperts, R. E. Stratmann, O. Yazyev, A. J. Austin, R. Cammi, C. Pomelli, J. W. Ochterski, R. L. Martin, K. Morokuma, V. G. Zakrzewski, G. A. Voth, P. Salvador, J. J. Dannenberg, S. Dapprich, A. D. Daniels, Ö. Farkas, J. B. Foresman, J. V. Ortiz, J. Cioslowski, D. J. Fox, Gaussian, Inc., Wallingford CT, 2009.

[S2] C. Adamo, V. Barone, *J Chem Phys,* 1999, **110**, 6158-6170.

[S3]M. Ernzerhof, GE. Scuseria, *J Chem Phys*, 1999,**110**, 5029.

[S4] A.D. Bochevarov, E. Harder, T.F. Hughes, J.R. Greenwood, D.A. Braden, D.M. Philipp, D. Rinaldo, M.D. Halls, J. Zhang, R.A. Friesner, *Int. J. Quantum Chem.*, 2013, **113**, 2110-2142.

[S4] Schrödinger Release 2016-4: Jaguar, Schrödinger, LLC, New York, NY, 2016.

[S6] P. Zarabadi-Poor, J. Barroso-Flores, *J. Phys. Chem. A*, 2014, **118**, 12178-12183.

[S7] C. Adamo, D. Jacquemin, *Chem Soc Rev.* 2013, **42**, 845-856.

4. Cell Study.

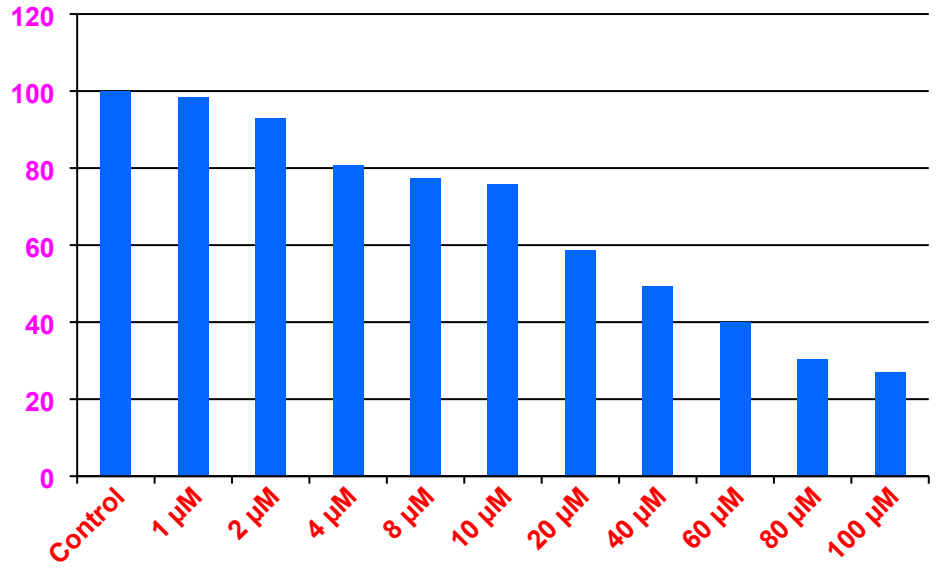

Figure S15. Percent (%) cell viability of HepG2 cells treated with different concentrations (1-100 µM) of **Hmppc** for 24 hours determined by MTT assay.